Probing Optical Anisotropy and Stability of $NbOCl_2$ and $NbOI_2$ using Mueller Matrix Spectroscopic Ellipsometry

Jianing Sun[a]*, Rafal Korlacki[a], Hong Liu[b,c,d], Ziyu Wang[b], Ruihuan Duan[c], and Zheng Liu[c]

[a] *J. A. Woollam company, Lincoln, NE, USA, 68508*

[b] *Institute of Materials Research and Engineering (IMRE), Agency for Science, Technology and Research (A*STAR), 2 Fusionopolis Way, #08-03, Innovis, Singapore 138634, Singapore*

[c] *School of Materials Science and Engineering, Nanyang Technological University, 50 Nanyang Avenue, Singapore 639798, Singapore*

[d] *Department of Materials Science and Engineering, National University of Singapore, 9 Engineering Drive 1, #03-09 EA, Singapore 117575, Singapore*

Keywords: *Niobium oxide dihalides, $NbOX_2$,* Mueller Matrix, *Ellipsometry, anisotropy, dielectric function, stability*

The niobium oxide dihalide family $NbOX_2$ (X = Cl, Br and I) exhibit strong in-plane anisotropy and hence polarization-dependent properties, making them great candidates for electronic, optoelectronic and quantum photonic applications. In this work the dielectric functions of $NbOCl_2$ and $NbOI_2$ nanoflakes were investigated using Mueller Matrix spectroscopic ellipsometry. Despite the monoclinic symmetry of the bulk materials, we propose a biaxial orthorhombic optical model and observe an excellent match to the ellipsometry data collected at different azimuth orientations. DFT calculations reveal that the principal axes of the dielectric tensor are indistinguishably close to the c and a* axis (the layer normal). Good agreement is also observed in the principal dielectric tensor obtained from DFT calculation and ellipsometry analysis. Onset of absorptions along the principal polar b-axis occur at higher energies compared to the non-polar c-axis, which defines the material bandgap of 1.75 eV for $NbOI_2$ and 2.1 eV for $NbOCl_2$ nanoflakes. The real part of the dielectric function tends to be higher for $NbOI_2$ than for $NbOCl_2$, in every principal direction. Remarkable linear dichroism was observed from UV to visible spectral range. $NbOCl_2$ remained optically stable in ambient storage while the optical properties of $NbOI_2$ changed dramatically over time, indicating material degradation under ambient conditions.

Niobium oxide dihalides $NbOX_2$ (X=*Cl, Br or I*) are newly emerged two-dimensional van der Waals (vdW) materials with both ferroelectric and antiferroelectric phases [1-5]. These transition metal compounds possess intrinsically high in-plane anisotropy [6-10], making them very promising candidates for high performance compact devices in optoelectronics and photonics. The oxyhalides have monoclinic crystal structure [11] (Figure 1a). The $NbOX_2$ monolayer sheets stack along the crystallographic *a*-axis in the out-of-plane direction. Nanoflakes are readily obtainable through mechanical exfoliation due to the weak interlayer electronic binding. The NbO_2X_4 octahedra are connected via edge sharing of halogen atoms along the *c*-axis. Importantly, the Nb-Nb dimers are off centered creating a first-order Peierls distortion [11]. Meanwhile, the Nb-O bonds align almost linearly along the *b*-axis with a second-order Peierls distortion [11], in which the adjacent Nb-O bonds are not equal in length. The distorted polar structure leads to ferroelectric polarization and remarkably high in-plane anisotropy. Understanding the polarizability and optical selectivity is important in guiding optical design and applications of niobium oxide dihalides, but

their dielectric functions, the fundamental material property directly describing the frequency and directional dependence of polarizability and loss are yet to be fully explored.

Several groups have calculated the anisotropic band structure of $NbOX_2$ using density functional theory (DFT) [1,4,12]. The approach provides insights into band dispersion, electron distribution and intrinsic anisotropic polarization. Jia et al [4] suggested absorption strength along c-axis is an order of magnitude higher relative to *b*-axis at 3.15eV in $NbOI_2$ monolayer. Guo et al. [12] observed unusually high contrast in the polarization-dependent transmission spectra of a thin $NbOCl_2$ nanoflake, with an almost complete extinction along the *c*-axis but up to 80% transmission along the *b*-axis.

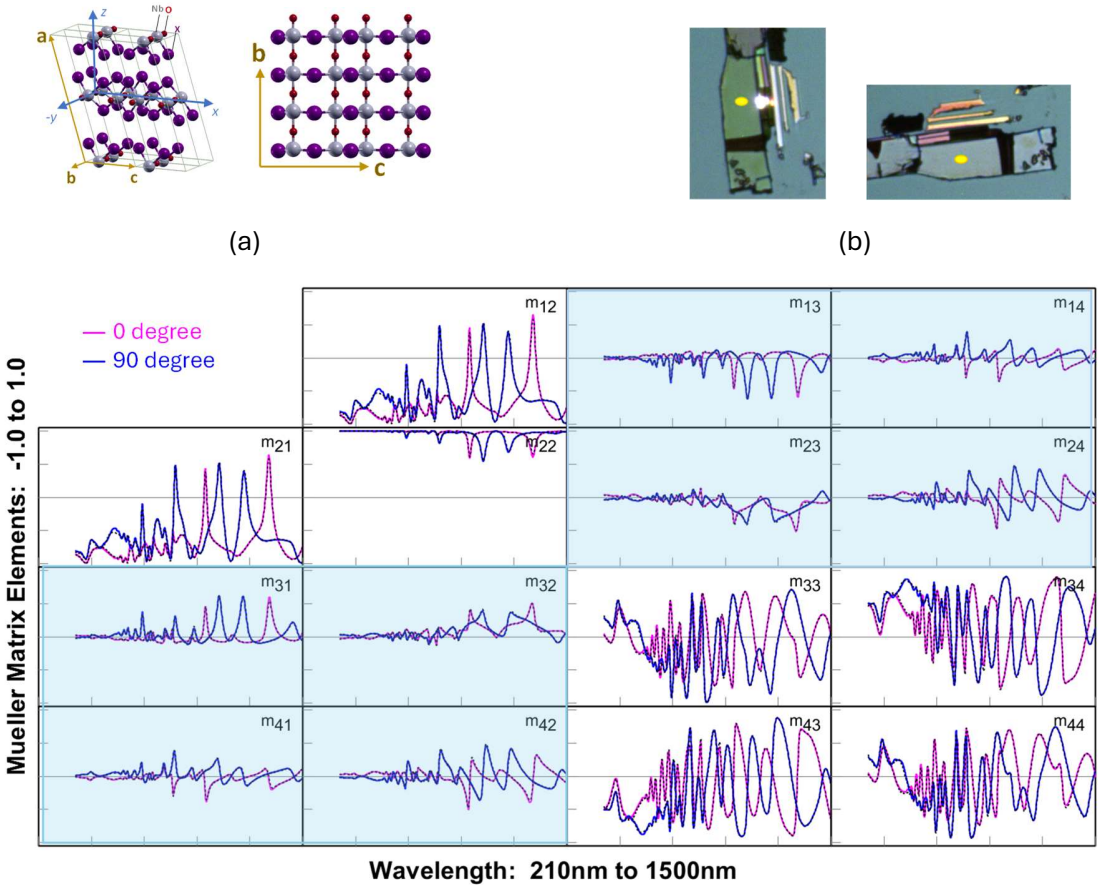

Figure 1 (a) Crystal structure of $NbOX_2$ in monoclinic symmetry, with b being the principal axis and van der Waals layers along a-axis. (b) Images of NbOI2 nanoflakes at two orientations, labeled as 0-degree and 90-degree. The ellipticals mark the ellipsometer beam position. (b) Mueller matrix data of $NbOI_2$ nanoflakes on 2 um thermal oxide on Si. Pink and Blue curves are experimental data at 0-degree and 90-degree, respectively. The dotted black lines from the biaxial optical model agree well with the experimental data.

Experimental methodology to reliably extract the complex dielectric functions of $NbOX_2$ nanoflakes is necessary and critical. However, very limited progress has been reported on this frontline and discrepancies exist between the DFT simulated and experimentally determined refractive index and bandgaps [1,4,12]. Optical characterization of these nanoflakes remains challenging due to the optical anisotropy, their complex band structure and the physical scale of existence. Generalized spectroscopic ellipsometry or Mueller Matrix ellipsometry [14-17] are proven optical approaches in characterizing low-symmetry anisotropic materials. Comprehensive characterization of monoclinic anisotropy requires multiple crystal orientations and measurements at different azimuth angles to resolve all of the independent dielectric function tensor elements [16, 18-20]. Considering the difficulties in achieving a 2nd complimentary crystal cut in these thin 2D vdW films, a reliable and precise technique that can overcome the availability limitation in facet cuts is required to determine the complex dielectric function. We applied Mueller matrix spectroscopic ellipsometry to $NbOCl_2$ and $NbOI_2$ nanoflakes. Herein an orthorhombic model is being proposed to analyze the polarization-dependent complex dielectric functions with discussion focusing on the in-plane dielectric functions. The effects of halogen atoms, film thickness and ambient exposure on the optical responses are investigated.

In order to further aid ellipsometry analysis, we performed DFT calculations in parallel with ellipsometry measurements using a plane-wave code Quantum ESPRESSO [21], generalized gradient approximation (GGA) density functional of Perdew, Burke, and Ernzerhof [22], and norm-conserving pseudopotentials from the SG15 distribution [23]. All calculations were performed with a high electronic wavefunction cutoff of 200 Ry. A dense shifted 8×8×8 Monkhorst-Pack [24] grid was used for sampling of the Brillouin zone and a convergence threshold of 10^{-12} Ry was used to reach self-consistency. The starting point of the calculations was the structure of $NbOI_2$ accompanying Ref. [1]. The structure was first relaxed to the force levels less than 10^{-5} Ry $Bohr^{-1}$ and the energy change less than 10^{-6} Ry. The equilibrium structure of $NbOI_2$ was used to model $NbOCl_2$, by replacing iodine atoms in the structure with chlorine atoms, and performing the structural relaxation again. The dielectric tensors and Born effective-charge tensors were calculated at the equilibrium geometries using density functional perturbation theory [25] as implemented in the Phonon code of Quantum ESPRESSO distribution.

Three nanoflakes were mechanically exfoliated from $NbOX_2$ (X=Cl and I) crystals and transferred onto a silicon substrate with 2 μm thermal oxide. The thickness of $NbOCl_2$, $NbOI_2$-thin and $NbOI_2$-thick are respectively 85nm, 65nm and 500 nm. Lateral dimensions of the flakes are up to a few hundred microns. The samples were originally sealed in a dry nitrogen filled bag and exposed to ambient environment since the initial ellipsometry measurement. A J.A. Woollam small spot RC2 ellipsometer (beam spot of 25um by 40um) was used to acquire the complete 4x4 Mueller Matrix data from 210 nm to 1500 nm at 65-degree angle of incidence. Data at two different azimuth orientations were collected. A sample was first measured at an arbitrary orientation, and the data was referred to as 0-degree. The sample was then rotated 90 degrees counterclockwise around the sample normal axis (Figure 1b). The second data acquired was referred to as 90-degree.

The Mueller Matrix spectroscopic data of the 500 nm $NbOI_2$ flake are shown in Figure 1c. Each plotted component was normalized to M11 element. The non-vanishing off-diagonal block components shaded in Figure 1c (m13, m14, m23, m24, m31, m32, m41 and m42) indicate the presence of cross-polarization. More prominently, the Mueller matrix data shows clear differences between 0-degree and 90-degree spectra. Similar phenomena were observed in the other flakes. The orientation dependence in raw data confirms the in-plane anisotropy [14-17].

A three-layer optical model ($NbOX_2/SiO_2/Si$) was developed to analyze the Mueller Matrix spectra. Published refractive index were adopted [26] for the silicon substrate and the underlayer thermal oxide. For very thin films, the optical response is less sensitive in the out-of-plane direction, which is in the monoclinic *ac* plane. We assumed orthorhombic biaxial anisotropy for the $NbOX_2$ films. The in-plane directions are along the principal b-axis and the crystalline c-axis. We label the out-of-plane direction perpendicular to the *bc* plane as *a** [27]. The complex dielectric functions along three principal axes were each described using Kramers-Kronig consistent Tauc-Lorentzian and Gaussian oscillators. Data collected at 0- and 90-degree orientations were analyzed simultaneously in determining the complex dielectric functions and flake thickness. The orientations were differentiated using the in-plane Euler angle Phi.

We found excellent agreement in Mueller Matrix elements simulated from the orthorhombic optical models and the spectroscopic ellipsometry data collected at both orientations (Figure 1c). The out-of-plane dielectric functions in a* direction are found to be low compared to *b*- and *c*-axis, as expected considering the separation between sheets in the general stacking direction. We further investigated the applicability of the orthorhombic approximation by checking the principal directions from DFT calculation. In monoclinic crystals, the principal directions of the dielectric tensor generally do not coincide with crystallographic directions within the monoclinic plane (*ac*) due to the low symmetry of the lattice (the symmetry axis *b* is always a principal direction) [28]. Diagonalizing the dielectric tensor obtained in DFT calculations reveals that in case of $NbOX_2$, the principal directions in the transparent region below bandgap align to within a fraction of a degree with the crystallographic axis *c* and direction perpendicular to the *bc* plane – the *a** axis. Thus, due to the highly organized arrangement of atoms within each layer, the dielectric tensor aligns almost perfectly with the Cartesian system used in the present work, which explains how our optical model can provide such a satisfactory description and underscores the feasibility of orthorhombic approximation in the optical analysis of $NbOX_2$ nanoflakes.

Neglecting phonon absorptions at low frequencies, we determined the principal dielectric tensor of ε_1 as energy approaches 0 eV. The extrapolated values compared with results obtained from DFT calculations are given in Table 1, showing remarkable agreement. There are small differences in experimental principal dielectric tensor values as film thickness changes.

Sample ID	Direction	SE	DFT (bulk)
$NbOCl_2$	*x (c)*	5.58	5.51
	y (b)	4.45	4.34
$NbOI_2$ 65nm / 500nm	*x (c)*	7.33 / 7.81	8.09
	y (b)	5.04 / 5.31	5.93

Table 1. Principal components of the transparent dielectric tensor.

The dielectric functions of the $NbOCl_2$ nanoflake and $NbOI_2$ nanoflakes are plotted in Figure 2a and 2b. The results are encouragingly in good agreement with the refractive index values extracted from transfer Matrix method and confirmed with the polarization dependent transmission spectra [12]. The imaginary dielectric functions of the two $NbOI_2$ nanoflakes have similar absorption profile, with the 500nm film showing better developed fine structure of absorption peaks, likely representative of the bulk material. Similar imaginary dielectric function ε_2 was reported in Ref [1] though we do not detect as strong absorption at ~2.3 eV along *c*-axis. In our Kramers-Kronig consistent analysis ε_2 approaches zero at low energies.

Two trends are evident from the plots of the dielectric functions: for each material studied, the real part of the dielectric function on the low-energy end of the spectral range (below the onset of absorptions) is higher along the *c* direction than along the symmetry axis *b*. Both values are higher for $NbOI_2$ than for $NbOCl_2$. In general, the level of ε_1 far below the bandgap reflects the total amount of absorptions present in the higher-energy absorbing region of a material (through the Kramers-Kronig relations). Iodide, with a higher atomic number, has more electrons than chlorine, and more electronic states producing absorbing optical band to band transitions, including above the spectral region studied here. Indeed, more absorptions in $NbOI_2$ are observed in the analyzed spectral range. The distribution of absorptions between specific directions, on the other hand, is determined by the curvature of bands involved in the transitions. Several broad absorptions are determined along the *c*-axis, while few peaks along the polar *b*-axis. The dielectric functions of $NbOCl_2$ have similar profile except the absorption peaks blue-shift to higher energies.

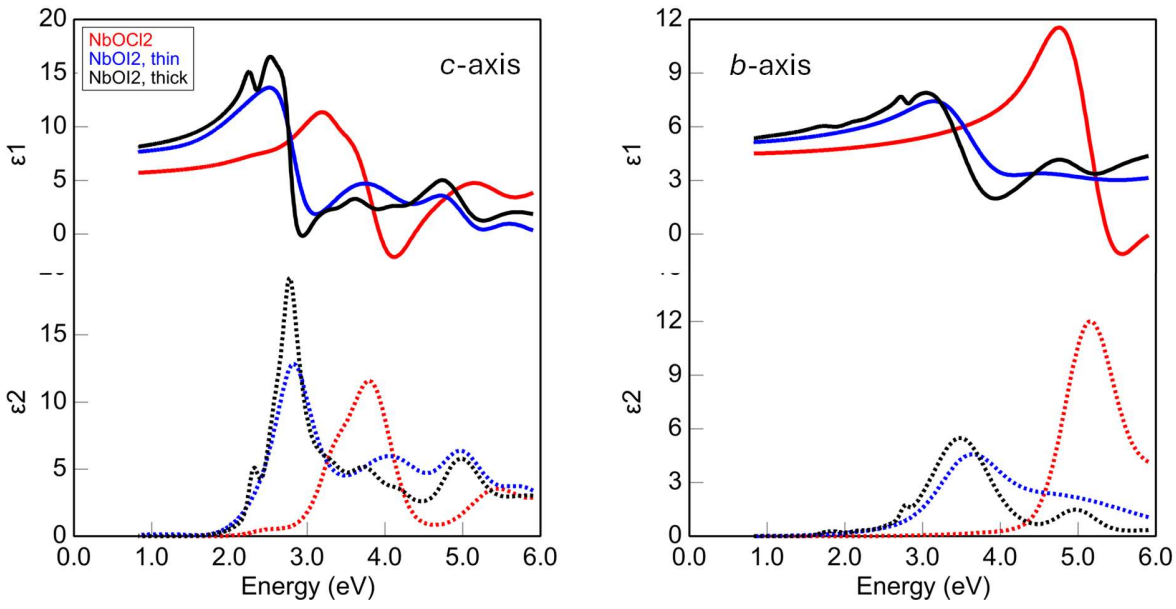

(a) (b)

Figure 2. Dielectric functions of $NbOCl_2$ (red) and $NbOI_2$ (thin-light blue, thick-dark blue) nanoflakes: (a) along the c-axis; (b) along the b-axis

To better understand the differences in optical absorption between the two materials we turn to their band structures, but the discussion of the band structure needs to start with the Brillouin zones (BZ). $NbOX_2$ have centered monoclinic lattice (space group No. 5) and their BZ is of $MCLC_1$-type, according to the classification of Setyawan and Curtarolo [29], as it was already reported by Jia *et al*. [4]. As such it is similar to the BZ for β-Ga_2O_3 discussed in detail by Mock *et al*. [20] and we plot the band structures using the high-symmetry path defined in Ref. 20. Note that the variables defining the reciprocal coordinates of some high symmetry points in Table I of Ref. 20 are structure-dependent and have different values for $NbOX_2$ than what was reported for β-Ga_2O_3.

The calculations of the band structures were performed using a hybrid density functional Gau-PBE [30-31] at the previously described PBE equilibrium geometries. For these calculations we used a regular non-shifted 8×8×8 Monkhorst-Pack grid for sampling of the Brillouin zone and 4×4×4 grid for sampling of the Fock operator. The kinetic energy cutoffs for the charge density and for the Fock operator were both set to 600 Ry The high-resolution interpolated band structure was obtained by utilizing the band interpolation method based on the maximally localized Wannier functions [32-33] as implemented in the software package WANNIER90 [34]. As the initial projections for the Wannier functions we used *p*-type states on O and halogen X atoms and *d*-type states on Nb atoms. 19 highest occupied (valence) bands and 9 lowest unoccupied (conduction) bands were included in the Wanier functions calculations.)

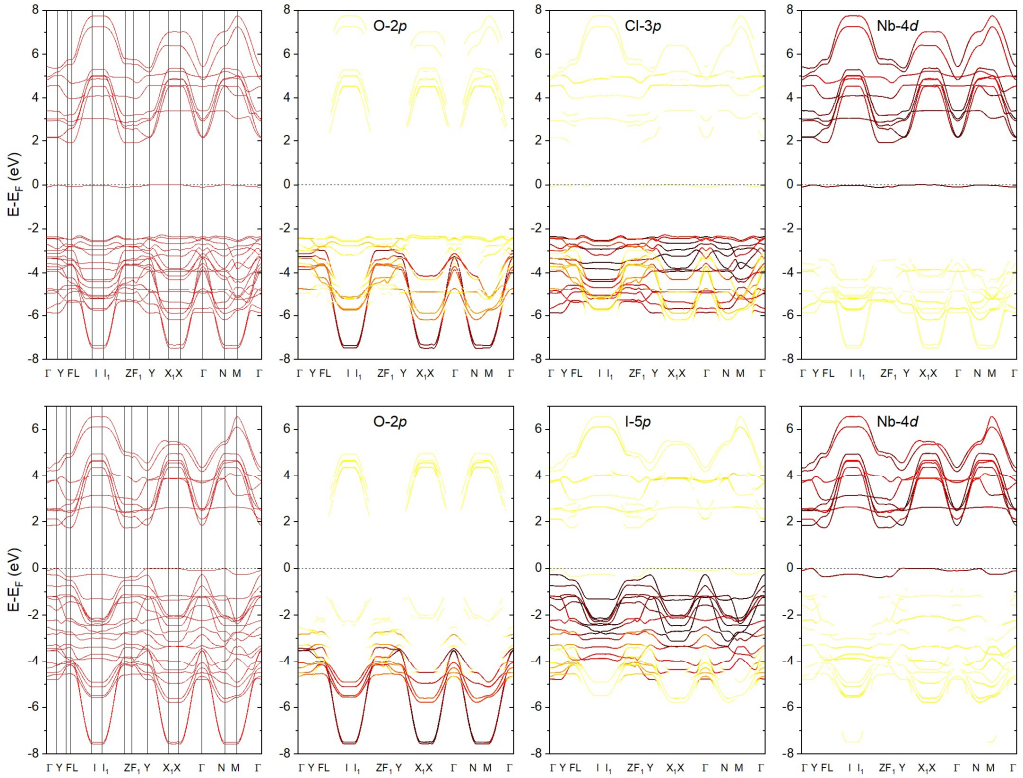

Figure 3. Band structure of NbOCl2 (upper row) and NbOI2 (lower row) calculated using the hybrid Gau-PBE density functional. In each row, color-coded plots present the energy bands projected onto localized atom-centered Wannier functions. Darker color means higher contribution with 10% increments.

Figure 3 shows the band structures of both niobates calculated using the hybrid Gau-PBE density functional. The band structures are consistent with the band structures reported by Jia *et al*. [4] [obtained using a different hybrid density functional (HSE)], except that we chose to include more high-symmetry lines in our path through the BZ. We can make several observations here. The bandgap for both materials is clearly indirect. While the conduction band has very well-defined parabolic shape at the BZ center (Γ), there are several points where the energy of the conduction band drops below that of Γ by 10s of meV. The top of the valence band, on the other hand is quite flat. Therefore, we expect many vertical band-to-band transitions occurring almost everywhere within the BZ with the absorption profile being the envelope of groups of such transitions rather than individual transitions that will not be distinguishable here. The lowest conduction bands are dominated by *d*-states on Nb. The highest single isolated valence band is also Nb-4*d*, identified by Jia et al. [4] as Nb-d_z^2. As the optical transitions require a change of angular momentum by ±1, we may expect a difference between the electronic bandgap (energy gap between the highest occupied and lowest unoccupied states) and the so called optical bandgap (lowest-energy allowed optical transition). However, as the projected bands in Figure 3 indicate a small contribution of

halogen (Cl and I) *p*-states to the top valence band, the optical transitions are allowed between the top valence band and the bottom of the conduction band albeit with low magnitudes. Therefore, based on the band structure, we expect to observe the onset of absorption, with a small amplitude, right above 2 eV for $NbOCl_2$ and right below 2 eV for $NbOI_2$, with the bulk of optical transitions between *p*-states in the valence band and *d*-states in the conduction band occurring at a significantly higher energy. The bulk of the valence bands formed by *p*-states on the anions lie immediately below the top valence band for $NbOI_2$, but approx. 1.5-2 eV deeper in the case of $NbOCl_2$, consistent with the observed shift to higher absorption energies for the latter. The bands with high contributions of *p*-states of iodine show higher curvatures than those of chlorine, thus are expected to produce more and stronger optical transitions, increasing the low-energy ε_1 values for $NbOI_2$. From ellipsometry analysis, we determined the bandgap of $NbOCl_2$ and $NbOI_2$ to be 2.1 eV and 1.75 eV, respectively. These results qualitatively agree very well with the DFT calculation and are comparable to reported values [2, 13].

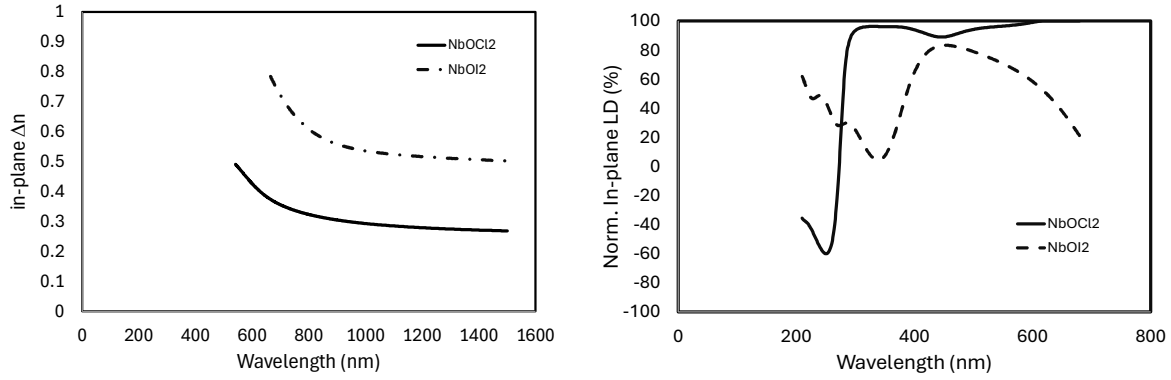

(a) (b)

Figure 4. In-plane refractive index of (a) NbOCl2; and (b) NbOI2; and comparison between NbOCl2 and NbOI2 nanoflakes (c) in-plane birefringence; and (d) normalized in-plane dichroism.

We define in-plane birefringence as:

$$\Delta n = n_c - n_b$$

where n_c and n_b are refractive indices in the *c* and *b* directions.

and normalized in-plane linear dichroism (nLD) as:

$$nLD = \frac{\alpha_c - \alpha_b}{\alpha_c + \alpha_b}$$

$$\alpha = \frac{4\pi k}{\lambda}$$

Where α is absorption coefficient, *k* is extinction coefficient and λ is wavelength.

We compare the in-plane birefringence and normalized in-plane linear dichroism of these materials at similar thickness, $NbOCl_2$ vs $NbOI_2$ thin (Figure 4a). Δn of $NbOCl_2$ almost reaches 0.5 in regions with no or low absorptions (k less than 0.05). The birefringence prevails even more in

the iodides, approaching 0.8. The in-plane refractive index difference of $NbOI_2$ remains over 0.5 while Δn of $NbOCl_2$ stays close to 0.3 in the visible to near infra-red range. $NbOCl_2$ is observed to have sharp dichroism transition below bandgap. Below 290 nm, the absorption dominates along the b-axis. It quickly switches to c-axis and reaches near unity linear dichroism above 300 nm. These findings are consistent with results in Ref. [12]. $NbOI_2$ presents high dichroism band absorptions favoring c-axis in both the visible and UV spectrum with nLD above 0.8 from 440 nm to 510 nm. These unusual anisotropic responses make such materials great candidates for polarizing optics or electrooptic devices.

As-synthesized bulk $NbOX_2$ crystals are reported stable in atmosphere [3]. We monitored the ambient stability of these nanoflakes. Data was collected on samples as obtained and again after one year. The Mueller Matrix spectra of $NbOCl_2$ barely changed (Figure 5a). Both orientations retained the data consistency, indicating ambient stability during the entire test period. Raw data of $NbOI_2$ after one year, however, become drastically different from the initial measurement comparing Figure 5b and Figure 1c. The off-diagonal Mueller Matrix elements become zero. Meanwhile, no noticeable differences are observed between the data collected at 0-degree and 90-degree, confirming the loss of in-plane anisotropy after the long ambient exposure. Chemical degradation due to moisture attack to the dangling iodine bonds was proposed in Ref. 35. The substantial changes in raw data validate ellipsometry as a direct approach monitoring the nanoflake stability and draw attention to resolutions in overcoming the stability issues in their long-term applications.

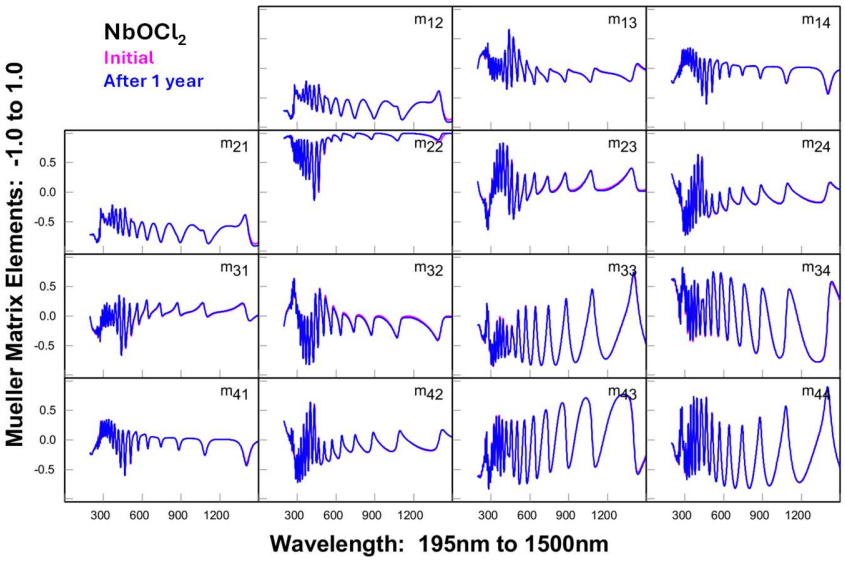

(a)

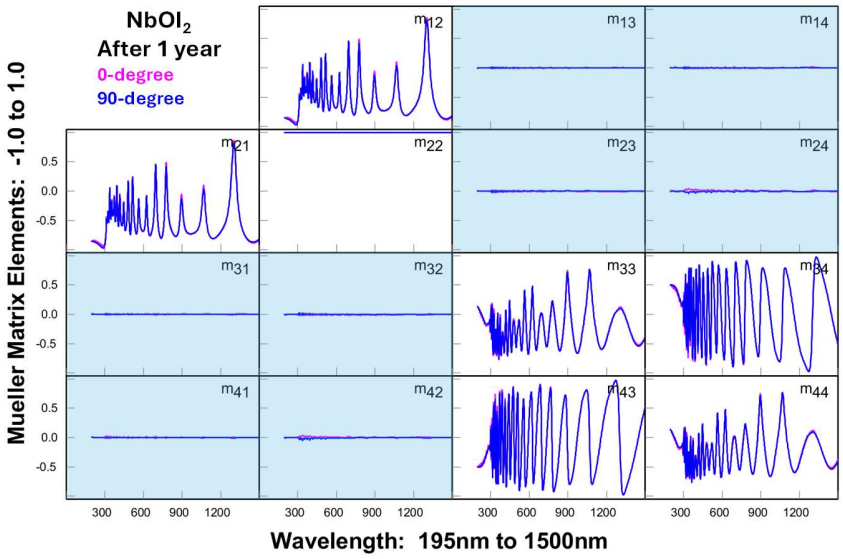

(b)

Figure 5. Ambient stability data: (a) Mueller matrix spectra of $NbOCl_2$ nanoflakes collected originally (pink) and after 1 year (cyan); (b) Mueller matrix spectra of $NbOI_2$ after 1 year

In summary, the low-symmetry polar structure of $NbOCl_2$ and $NbOI_2$ nanoflakes leads to strong in-plane anisotropy along the b and c directions. We determined their optical properties using Mueller Matrix spectroscopic ellipsometry. The assumed orthorhombic anisotropy focuses the analysis on the significant in-plane optical responses and provides a reasonable approximation in determining the dielectric functions of these thin 2D films, grounded in their microscopic structure and supported by first-principles calculations. $NbOI_2$ is found to have higher birefringence in the visible and near infrared spectral range while $NbOCl_2$ presents near unity dichroism in the UV range. The optical bandgap of $NbOCl_2$ and $NbOI_2$ was determined to be 1.75 eV and 2.1 eV respectively along the non-polar *c*-axis. The observed indications of chemical degradation of $NbOI_2$ under ambient conditions emphasize the importance of long-term stability. These findings in the $NbOX_2$ optical behaviors will provide insights into future exploration of these 2D van der Waals materials in high performance optical, energy harvesting and sensing devices.

Authors Contributions

H. Liu and Z. Liu were involved in technical discussions and manuscript drafting. Z. Wang and R. Duan perform the sample preparation.

Email address

Ziyu Wang: wang_ziyu@a-star.edu.sg

Hong Liu: liu_hong@a-star.edu.sg

Ruihuan Duan: Ruihuan.duan@ntu.edu.sg

Zheng Liu: z.liu@ntu.edu.sg

Acknowledgement

H. Liu and Z. Liu acknowledge the support from National Research Foundation Competitive Research Programme (CRP) funding of Singapore under award no. NRF-CRP31-0001 and the RIE2025 Manufacturing, Trade and Connectivity (MTC) Programmatic Fund (M23M2b0056). H. Liu acknowledges RIE2025 MTC Individual Research Grants (IRG) (M24N7c0087). Z. Liu acknowledges supports from Singapore National Research Foundation–Competitive Research Program NRF-CRP22-2019-0007, and NRF-CRP264-2021-0004. This research is also supported by the Singapore Ministry of Education Tier 3 and Tier 2 Programmatic Fund (award no. MOEMOET32023-0003, and MOE-T2EP50223-0008) and the Singapore Ministry of Education Academic Research Fund (AcRF) Tier 1 (award no. 023785-00001). R. Duan acknowledges support from the Agency for Science, Technology and Research (A*STAR) under the MTC Young Individual Research Grants (YIRG) (M24N8c0097).

References

[1] I. Abdelwahab, B. Tilmann, Y. Zu, D. Giovanni, I. Verzhbitskiy, M. Zhu, R. Berte, F. Xuan, L. d S. Menezes, G. Eda, T. C. Sum, S. Y. Quek, S. A. Maier and K. P. Loh, *Nature Photonics* **16**, 644 (2022)

[2] Q. Guo, X. Z. Qi, L. Zhang, M. Gao, S. Hu, W. Zhou, W. Zang, X. Zhao, J. Wang, B. Yan, M. Xu, Y.-K. Wu, G. Eda, Z. Xiao, S. A. Yang, H. Gou, Y. P. Feng, G.-C. Guo, W. Zhou, X.-F. Renh, C. -W. Qiu, S. J. Pennycook and A. T. S. Wee, *Nature* **613**, 53 (2023)

[3] X. Sun, Y. Wan, Y. Fang and F. Huang, *Small Sci.* **4**, 2300125 (2024)

[4] Jia Y., Zhao M., Gou G., Zeng X. C., and Li J., *Nanoscale Horiz.* **4**, 1113 (2019)

[5] Y. Wu, I. Abdelwahab, K. C. Kwon, I. Verzhbitskiy, L. Wang, W. H. Liew, K. Yao, G. Eda, K. P. Loh, L. Shen and S. Y. Quek, *Nature Communications* **13**, 1884 (2022)

[6] L. Ye, W. Zhou, D. Huang, X. Jiang, Q. Guo, X. Cao, S. Yan, X. Wang, D. Jia, D. Jiang, Y. Wang, X. Wu, X. Zhang, Y. Li, H. Lei, H. Gou and B. Huang, *Nature Communications* **14**, 5911 (2023)

[7] H. Wang, Q. Chen, Y. Cao, W. Sang, F. Tan, H. Li, T. Wang, Y. Gan, D. Xiang and T. Liu, *Nano Lett.* **24**, 3413 (2024)

[8] W. Chen, S. Zhu, R. Duan, C. Wang, F. Wang, Y. Wu, M. Dai, J. Cui, S. H. Chae, Z. Li, X. Ma, Q. Wang, Z. Liu and Q. J. Wang, *Adv. Mater.* **36**, 2400858 (2024)

[9] L. Kallioniemi, X. Lyu, R. He, A. Rasmita, R. Duan, Z. Liu and W. Gao, *Nature Photonics* **19**, 142 (2025), https://doi.org/10.1038/s41566-024-01545-5

[10] Q. Guo, Y.-K. Wu, D. Zhang, Q. Zhang, G.-C. Guo, A. Alu, X.-F. Ren and C.-W. Qiu, *Nature Communications* **15**, 10461 (2024)

[11] J. Beck and Ch., Z. Kusterer, *Anorg. Allg. Chem.* **632**, 2193 (2006)

[12] Q. Guo, Q. Zhang, T. Zhang, J. Zhou, S. Xiao, S. Wang, Y. P. Feng and C.-W. Qiu, *Nature Photonics* **18,** 1170 (2024).

[13] Y. Fang, F. Wang, R. Wang, T. Zhai and F. Huang, *Adv. Mater.* **33**, 2101505 (2021)

[14] G. E. Jellison, *Thin Solid Films* **450**, 42 (2004)

[15] H. Fujiwara, Spectroscopic Ellipsometry: Principles and Applications (John Wiley & Sons, 2007).

[16] M. Schubert, R. Korlacki, S. Knight, T. Hofmann, S. Schoeche, V. Darakchieva, E. Janzen, B. Monemar, D. Gogova, Q.-T. Thieu, R. Togashi, H. Murakami, Y. Kumagai, K. Goto, A. Kuramata, S. Yamakoshi and M. Higashiwaki, *Phys. Rev. B* **93**, 125209 (2016)

[17] J.N. Hilfiker, N. Hong, and S. Schoeche, *Adv. Opt. Techn.* **11**, 59 (2022)

[18] C. Sturm, J. Furthmuller, F. Bechstedt, R. Schmidt-Grund and M. Grundmann, *APL Materials* **3**, 106106 (2015)

[19] C. Sturm, R. Schmidt-Grund, C. Kranert, J. Furthmüller, F. Bechstedt, and M. Grundmann, *Phys. Rev. B* **94**, 035148 (2016)

[20] A. Mock, R. Korlacki, C. Briley, V. Darakchieva, B. Monemar, Y. Kumagai, K. Goto, M. Higashiwaki and M. Schubert, *Phys. Rev. B* **96**, 245205 (2017)

[21] P. Giannozzi, S. Baroni, N. Bonini, M. Calandra, R. Car, C. Cavazzoni, D. Ceresoli, G. L. Chiarotti, M. Cococcioni, I. Dabo, A. D. Corso, S. de Gironcoli, S. Fabris, G. Fratesi, R. Gebauer, U. Gerstmann, C. Gougoussis, A. Kokalj, M. Lazzeri, L. Martin-Samos, N. Marzari, F. Mauri, R. Mazzarello, S. Paolini, A. Pasquarello, L. Paulatto, C. Sbraccia, S. Scandolo, G. Sclauzero, A. P. Seitsonen, A. Smogunov, P. Umari, and R. M. Wentzcovitch, *J. Phys.: Condens. Mater* **21**, 395502 (2009)

[22] J. P. Perdew, K. Burke, and M. Ernzerhof, *Phys. Rev. Lett.* **77**, 3865 (1996)

[23] M. Schlipf and F. Gygi, *Comput. Phys. Commun.* **196**, 36 (2015).

[24] H. J. Monkhorst and J. D. Pack, *Phys. Rev. B* **13**, 5188 (1976).

[25] X. Gonze and Ch. Lee, *Phys. Rev. B* **55**, 10355 (1997)

[26] C.M. Herzinger, B. Johs, W.A. McGahan, J.A. Woollam and W. Paulson, *J. Appl. Phys.* **83**, 6, 3323 (1998)

[27] P. Gopalan, S. Knight, A. Chanana, M. Stokey, P. Ranga, M. A. Scarpulla, S. Krishnamoorthy, V. Darakchieva, Z. Galazka, K. Irmscher, A. Fiedler, S. Blair, M. Schubert, and B. Sensale-Rodriguez, *Appl. Phys. Lett.* **117**, 252103 (2020)

[28] C. Traum, P. L. Inácio, C. Félix, P. Segonds, A. Peña, J. Debray, B. Boulanger, Y. Petit, D. Rytz, G. Montemezzani, P. Goldner, and A. Ferrier, *Opt. Mater. Exp.* **4**, 57 (2013)

[29] W. Setyawan and S. Curtarolo, *Comput. Mater. Sci.* **49**, 299 (2010).

[30] J.-W. Song, K. Yamashita, and K. Hirao, *J. Chem. Phys.* **135**, 071103 (2011).

[31] J.-W. Song, G. Giorgi, K. Yamashita, and K. Hirao, *J. Chem. Phys.* **138**, 241101 (2013).

[32] N. Marzari and D. Vanderbilt, *Phys. Rev. B* **56**, 12847 (1997).

[33] I. Souza, N. Marzari, and D. Vanderbilt, *Phys. Rev. B* **65**, 035109 (2001).

[34] G. Pizzi, V. Vitale, R. Arita, S. Blügel, F. Freimuth, G. Géranton, M. Gibertini, D. Gresch, C. Johnson, T. Koretsune, J. Ibañez-Azpiroz, H. Lee, J.-M. Lihm, D. Marchand, A. Marrazzo, Y. Mokrousov, J. I. Mustafa, Y. Nohara, Y. Nomura, L. Paulatto, S. Poncé, T. Ponweiser, J. Qiao, F. Thöle, S. S Tsirkin, M. Wierzbowska, N. Marzari, D. Vanderbilt, I. Souza, A. A Mostofi, and J. R Yates, *J. Phys.: Condens. Matter* **32** 165902 (2020)

[35] Q. Yan, Y. Weng, S. Wang, Z. Zhou, Y. Hu, Q. Li, J. Xue, Z. Feng, Z. Luo, R. Feng, L. You and L. Fang, *ACS Appl. Mater. Interfaces* **16**, 9051 (2024)